# Computational study of hydrogen bond interactions in water cluster-organic molecule complexes

Eduardo Romero-Montalvo[†] and Gino A. DiLabio[*,†,‡]

†*Department of Chemistry, University of British Columbia, 3247 University Way, Kelowna, British Columbia, Canada V1V 1V7*

‡*Faculty of Management, University of British Columbia, 1137 Alumni Avenue, Kelowna, British Columbia, Canada V1V 1V7*

E-mail: gino.dilabio@ubc.ca

**Abstract**

We analyzed the interactions present in complexes that acetone, azomethane, dimethylamine, dimethyl ether, methyl acetate, and oxirane form with 39 different $(H_2O)_n$ clusters (n=1-10). A random generation of configurations and a subsequent screening procedure were employed to sample representative interactions. Using quantum chemical computations, we calculated the associated binding energies, ranging from -0.19 kcal/mol to -10.76 kcal/mol at the DLPNO-CCSD(T)/CBS level. It was found that this set of energies is diverse and can be elucidated in terms of various factors, including the water cluster size, the nature of the organic molecule, and type of hydrogen bond donor. We find that the most stable complexes often arise from a combination of a strong hydrogen bond plus a secondary interaction between the organic molecule and the water cluster.

# 1 Introduction

Water can be used as a reaction medium in organic chemistry. Diels and Alder mixed furan and maleic anhydride in hot water, obtaining a cycloaddition adduct with an increased endo-selectivity compared to their organic solvent counterpart.[1] However, it was not until the 1980s that a systematic and pioneering series of papers by Breslow and coworkers established the paradigm of water as useful and relevant in organic chemistry. In their research, it was demonstrated that $H_2O$ as a solvent increases the reaction rate of Diels-Alder reactions 700-fold, compared to reactions in organic solvents, mainly due to hydrophobic effects.[2–5] Breslow's seminal contributions set the foundations of aqueous organic chemistry (AOC) as a new field of research that is highly active today.[6–8] One of the key areas of activity is developing chemical procedures that reduce organic solvent usage in favour of $H_2O$;[9,10] the non-toxicity, reusability, and low-cost of water perfectly align with the principles of green chemistry.[11] It is expected that further expanding research in AOC will lead to significant discoveries in chemistry.

Understanding hydrogen bonding (HB) interactions between organic molecules and water molecules is central to unravel the poorly understood mechanisms of AOC. For example, it has been proposed that a group of accelerated reactions in aqueous emulsions, called "on water" reactions, occurs due to HB stabilization of transition states relative to reactants.[12] Also, countless chemical processes relevant to biology involve HBs between water molecules and organic substrates.[13–19] In light of the importance of organic molecule-water cluster bonding, the present work focuses on the accurate quantum mechanical description of such interactions.

HB interactions within water clusters have been extensively studied over the past decades. It is a well-known fact that cooperative effects are prominent in these interactions[20–24] and that they increase with the number of water molecules in the cluster. In addition to the cluster size, the local environment of hydrogen bonds is relevant; the nature of the HB donor and acceptor and their neighbouring molecules has been used to describe noncovalent

interactions within water clusters of small size.[25,26] However, to the best of our knowledge, a comprehensive work on organic molecule interactions with water clusters of distinct sizes has not yet been explored. Some computational studies have shown that density functional theory (DFT) can reproduce experimental results in AOC reactions.[12,27,28] However, most quantum chemistry models utilize only a few water molecules to represent the complex traits of HB in these systems, completely neglecting the role of water cluster size in accurately depicting hydrogen bonding interactions with organic molecules. For these reasons, in this work, we explore the interaction strengths of water clusters of varying sizes with organic HB acceptors. In the process of our study, we developed a new benchmark data set of hydrogen bonding for organic molecule-water cluster complexes.

## 2 Computational Methods

An accurate quantum chemical description of water systems can only be achieved for small water clusters.[29,30] These limitations demand that we approximate our molecular systems with small models. Despite their reduced size, model systems can often produce insightful information for a variety of chemical problems. For our study, we wanted to understand the behaviour of binding energies between organic molecules and water clusters of increasing size. For this purpose, we retrieved the water clusters produced by Temelso and coworkers[31] that range in size from the monomer to the decamer. A summary of the structures studied in this paper is shown in Table 1, and an example of them is displayed in Figure 1. Temelso et al. obtained these structures at the RI-MP2[32,33]/aug-cc-pVDZ[34] level of theory, making them appropriate for benchmarking purposes. We also selected the following seven organic molecules as representative of species that are present in AOC reactions: acetone, dimethyl ether, oxirane, methyl acetate, azomethane, dimethylamine, and trimethylamine, which we pre-optimized at B3LYP[35–37]/6-31+G** using Gaussian 16 (g16).[38] This selection was based on their similarity to organic substrates involved in "on water" reactions.[39] We used these

organic molecules as probes to study the HB donating capabilities of −OH groups in small water clusters. For the sake of simplicity, we will often refer to these organic molecules as *probes* in this work.

Table 1: Names of the water clusters considered in this work. The structures of all oligomers of water shown here can be seen in Figures 1 and 2 of reference 31.

| Cluster size, n | Labels |
|---|---|
| 1 | Monomer |
| 2 | 2Cs |
| 3 | 3UUD, 3UUU |
| 4 | 4Ci, 4PY, 4S4 |
| 5 | 5CA-A, 5CA-B, 5CA-C, 5CYC, 5FR-A, 5FR-B, 5FR-C |
| 6 | 6BAG, 6BK-1, 6BK-2, 6CA, 6CB-1, 6CB-2, 6CC, 6PR |
| 7 | 7BI1, 7BI2, 7CA1, 7CA2, 7CH1, 7CH2, 7CH3, 7HM1, 7PR1, 7PR2, 7PR3 |
| 8 | 8D2d, 8S4 |
| 9 | 9D2dDD, 9S4DA |
| 10 | 10PP1, 10PP2 |

The complexes formed by the interactions between the probes and water clusters of

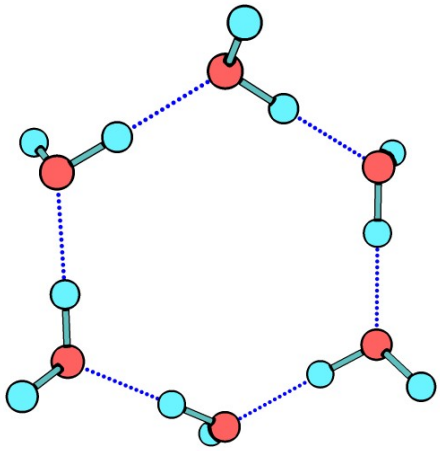

Figure 1: Hexamer (6CC) of water. Colour code, red: oxygen, and blue: hydrogen. Dashed lines indicate HB interactions.

various sizes could take on any one of a large number of configurations: as water cluster sizes increase, so does the number of available −OH donor groups with which the acceptors can interact. To explore different complexes, we fixed the coordinates of the water clusters and allowed the pre-optimized probes to freely move around the water clusters using a random generator of coordinates to obtain 2000 structures per water cluster-probe complex, followed by an approach with intermediate computational expense steps to refine the data set. The module genmer from the Molclus software[40] was employed to generate the 2000 configurations for each complex. Next, we performed single-point (SP) calculations on these geometries and energy-ranked them using the UFF force-field,[41] and eliminated the 1000 least stable complexes (step I). In step II, we computed the single-point energy of the remaining 1000 compounds using HF-D3(BJ)/MINIs-ACP and reordering the structures based on electronic energy. The 500 least stable structures were removed from the list. Step III involved calculating the single-point energies of the remaining 500 complexes using B3LYP-D3(BJ)/6-31+G(d,p)-BSIP, reordering the structures by energy, and eliminating the 250 least stable structures. Step II employs atom-centered potentials (ACPs) that are designed to mitigate the effects of incomplete correlation and incomplete basis sets associated with the HF-D3(BJ)/MINIs approach.[42] Step III uses a form of ACPs called basis set incompleteness

potentials (BSIPs) designed to reduce the effects of incomplete basis sets used with conventional density-functional theory (DFT) based methods.[43] Steps I-III employed g16, and the process is summarized in Figure 2.

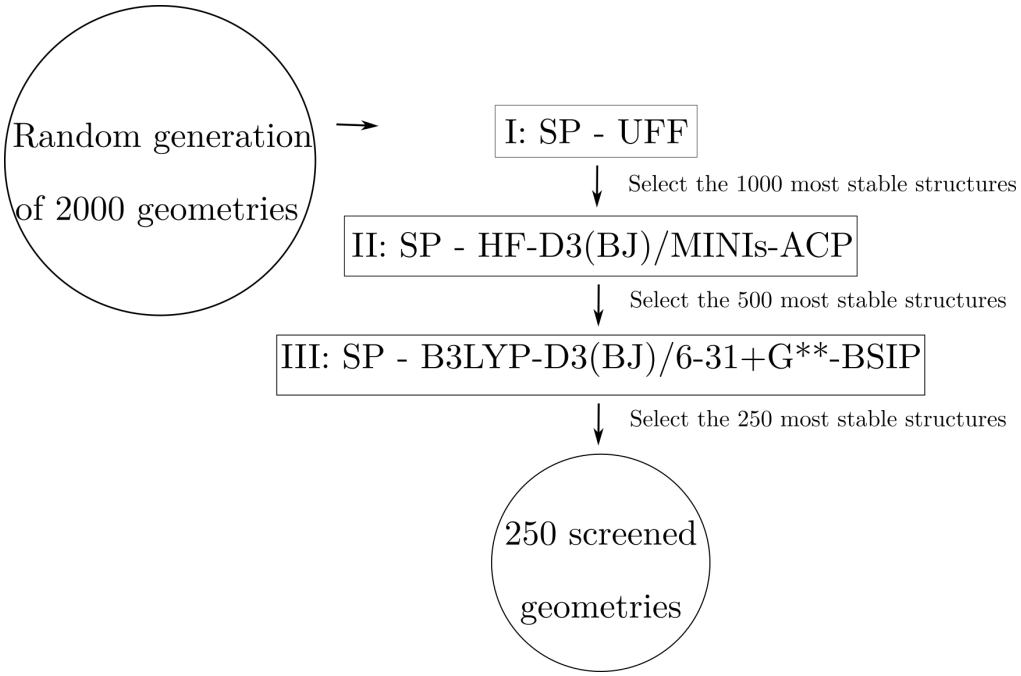


Figure 2: Summary of the screening process followed in selecting the most stable complexes formed between water clusters and the probes. We applied this procedure to each of the possible 273 complexes (7 probes interacting with 39 water clusters).

Following the foregoing screening, a set of 250 configurations per water cluster-probe complex was obtained. These energy-ranked configurations were divided into ten bins containing 25 conformers each. We then selected the most stable complex from each bin to get 10 structures per complex and re-optimized the geometries of the probes within the complexes at B3LYP-D3(BJ)[35–37,44–47]/6-31+G**-BSIP[43] using g16; in all cases, the structures of the water clusters were kept fixed at the Temelso geometries.[31] This approach has the advantage of using high-level geometries; however, since they are fixed structures, the donating $-$OH group in the water clusters will not relax and, hence, the binding energies we calculate will all be upper bounds. The resulting structures constitute the set of complexes for our benchmark calculations. We obtained 2730 complex structures in total.

From our 2730 geometries, we removed the redundant geometries that arose from config-

urations that converged to identical geometries when re-optimizing the probes in the complexes. For doing so, the COMPARE feature, as implemented in the program Critic2,[48,49] was employed. The final dataset contains 2376 non-redundant geometries. Our screening method ensured that strong interactions from the dangling −OH to the organic probes were present and other weaker interactions such as those involving C−H HB donors and dispersion interactions. The molecular systems were visualized using the software Chemcraft.[50]

Reference binding energy calculations were calculated using DLPNO-CCSD(T)[51] with aug-cc-pVDZ and aug-cc-pVTZ basis sets,[34] (represented as DZ and TZ, respectively). A strategy similar to the one presented in reference 52 was applied for the extrapolation to the complete basis set (CBS) limit: we calculated the counterpoise (CP) corrected binding energies ($\mathrm{BE_{CP}}$)[53,54] of the complexes as

$$\begin{aligned}\mathrm{BE_{CP}} = &\left[E^{\mathrm{Complex}}_{\mathrm{Complex}}\left(\mathrm{Complex}\right) - E^{\mathrm{Complex}}_{\mathrm{Complex}}\left(\left(\mathrm{H_2O}\right)_{\mathrm{n}}\right) - E^{\mathrm{Complex}}_{\mathrm{Complex}}\left(\mathrm{R}\right)\right] \\ &+ \left[E^{\left(\mathrm{H_2O}\right)_{\mathrm{n}}}_{\mathrm{Complex}}\left(\left(\mathrm{H_2O}\right)_{\mathrm{n}}\right) - E^{\left(\mathrm{H_2O}\right)_{\mathrm{n}}}_{\left(\mathrm{H_2O}\right)_{\mathrm{n}}}\left(\left(\mathrm{H_2O}\right)_{\mathrm{n}}\right)\right] + \left[E^{\mathrm{R}}_{\mathrm{Complex}}\left(\mathrm{R}\right) - E^{\mathrm{R}}_{\mathrm{R}}\left(\mathrm{R}\right)\right],\end{aligned} \tag{1}$$

where the general nomenclature, $E^{basis}_{\mathrm{geometry}}\left(X\right)$, represents the electronic energy of species X (R for probe, $\left(\mathrm{H_2O}\right)_{\mathrm{n}}$ for a water cluster of size n, and complex for the water cluster-probe aggregates), at the geometry specified by the subscript and using the basis set identified by the superscript. For example, the term $E^{\mathrm{R}}_{\mathrm{Complex}}\left(\mathrm{R}\right)$ represents the electronic energy of a probe at its geometry in a complex using the probe basis sets. Note that Equation 1 can be written alternatively as

$$\mathrm{BE_{CP}} = E^{\mathrm{CP}}_{\mathrm{int}}\left(\mathrm{Complex}\right) + E^{\mathrm{R}}_{\mathrm{def}}\left(\mathrm{R}\right), \tag{2}$$

in which $E^{\mathrm{CP}}_{\mathrm{int}}\left(\mathrm{Complex}\right) = E^{\mathrm{Complex}}_{\mathrm{Complex}}\left(\mathrm{Complex}\right) - E^{\mathrm{Complex}}_{\mathrm{Complex}}\left(\left(\mathrm{H_2O}\right)_{\mathrm{n}}\right) - E^{\mathrm{Complex}}_{\mathrm{Complex}}\left(\mathrm{R}\right)$, and the deformation energy of the organic probe, $E^{\mathrm{R}}_{\mathrm{def}}\left(\mathrm{R}\right)$ equals $E^{\mathrm{R}}_{\mathrm{Complex}}\left(\mathrm{R}\right) - E^{\mathrm{R}}_{\mathrm{R}}\left(\mathrm{R}\right)$. The deformation energies of the water clusters are zero because we are using frozen geometries for those structures, throughout. The non-counterpoise (non-CP) energies ($\Delta E^{\mathrm{non-CP}}_{\mathrm{BE}}$) are

defined by

$$\mathrm{BE}_{\mathrm{non-CP}} = E^{\mathrm{Complex}}_{\mathrm{Complex}}\left(\mathrm{Complex}\right) - \left[E^{(\mathrm{H_2O})_\mathrm{n}}_{(\mathrm{H_2O})_\mathrm{n}}\left((\mathrm{H_2O})_\mathrm{n}\right) + E^{\mathrm{R}}_{\mathrm{R}}\left(\mathrm{R}\right)\right]. \tag{3}$$

The ORCA[55] package was used for the DLPNO-CCSD(T) calculations. Equations 2 and 3 were evaluated for both basis sets, DZ and TZ. A two-point extrapolation (DZ-TZ) to the CBS limit was applied, as described in reference 56. We also computed the average of the CP and non-CP approaches as $\mathrm{BE}^{\mathrm{i}}_{\mathrm{ave}} = \left(\mathrm{BE}^{\mathrm{i}}_{\mathrm{CP}} + \mathrm{BE}^{\mathrm{i}}_{\mathrm{non-CP}}\right)/2$, with i = DZ, TZ, and DZ-TZ. We defined our benchmark binding energies as the average of the CP and non-CP energies at the CBS extrapolation limit (i = DZ-TZ). Mackie and DiLabio showed that CP BEs tend to converge to the complete basis set limit from above, while the non-CP BEs converge from below.[52] Therefore, averaging the two quantities generally results in quicker convergence to the CBS limit. These average binding energies show a quick convergence to the CBS limit for most noncovalent interactions studied herein. A selected example of the convergence of $\mathrm{BE}^{\mathrm{i}}_{\mathrm{ave}}$ is depicted in Figure 3; since $\mathrm{BE}_{\mathrm{CP}}$ and $\mathrm{BE}_{\mathrm{non-CP}}$ converge to the same value at the CBS limit (see right-hand sides of equations 1 and 3), $\mathrm{BE}^{\mathrm{i}}_{\mathrm{ave}}$ will more rapidly converge to the complete basis set limit than the individual counterpoise and non-counterpoise binding energies. However, the convergence of the average of the CP and non-CP BEs is not always ideal, i.e., when the CP and non-CP BEs do not converge from above or below, respectively. Figure 4 shows one of those examples in which the binding energies of a complex formed between azomethane and the hexamer 6CC are displayed. For this example, the non-CP binding energies show little variation with basis set. Nevertheless, more than 97% of the 2376 BEs we calculated show better convergence of the averaged BEs than the CP and non-CP BEs. The complete set of graphs showing the CBS extrapolation limit for all complexes is included in the Supporting Information (SI).

With our benchmark binding energy calculations in hand, we assessed the performance of a cross-section of density functional theory methods[57–65] and plotted the results in Figure

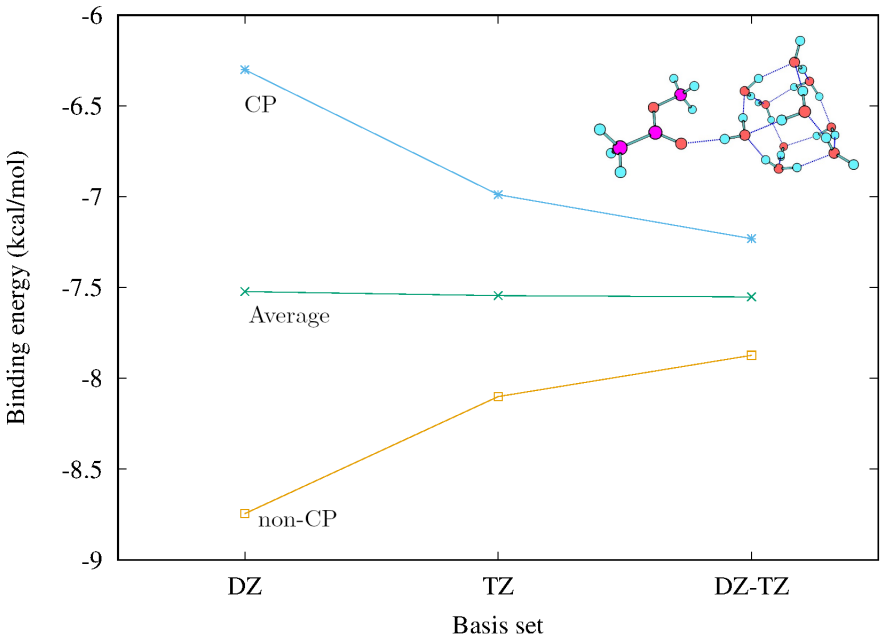


Figure 3: Two-point extrapolation to the CBS extrapolation limit for one of the binding energies between the decamer 10PP2 and methyl acetate. Our benchmark binding energies are the average of the CP and non-CP binding energies at the CBS extrapolation limit (DZ-TZ). Colour code, red: oxygen, blue: hydrogen, and magenta: carbon. Dashed lines indicate HB interactions.

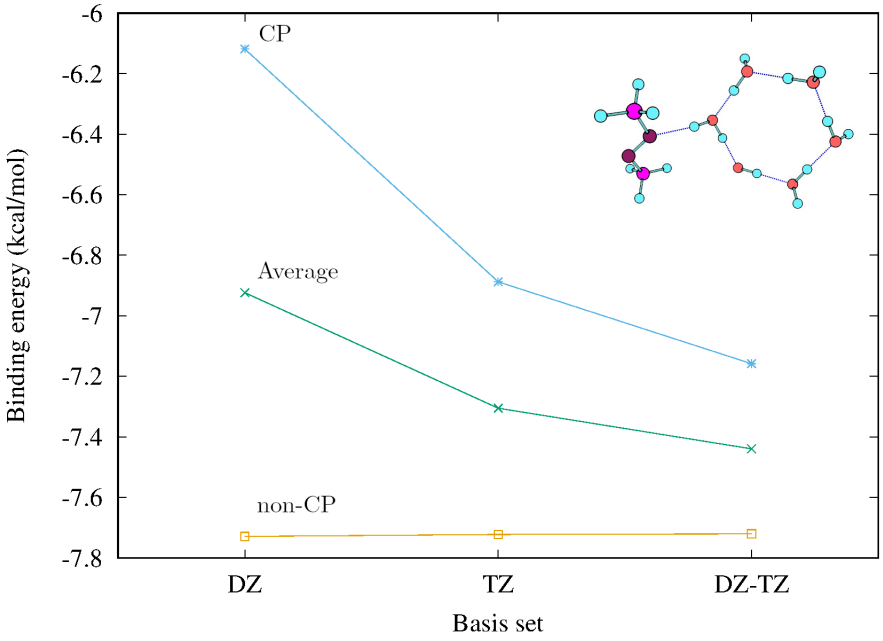


Figure 4: Two-point extrapolation to the CBS limit for one of the binding energies between the hexamer 6CC and azomethane. Our benchmark binding energies are the average of the CP and non-CP binding energies at the CBS extrapolation limit (DZ-TZ). Colour code, red: oxygen, blue: hydrogen, magenta: carbon, and maroon: nitrogen. Dashed lines indicate HB interactions.

5. This graph shows the mean absolute error (MAE) for each DFT approach; B3LYP-D3(BJ)/6-31+G**-BSIP, which we used as part of our procedure to generate the complex structures, has a 0.44 kcal/mol MAE value, which suggests that the method was suitable for the geometry optimization step of our calculations. We also note that BLYP-D3(BJ)/6-31+G**-BSIP and M05/6-31+G** reproduce the binding energies most closely amongst all of the DFT approaches assessed (MAEs of 0.25 and 0.26 kcal/mol, respectively).

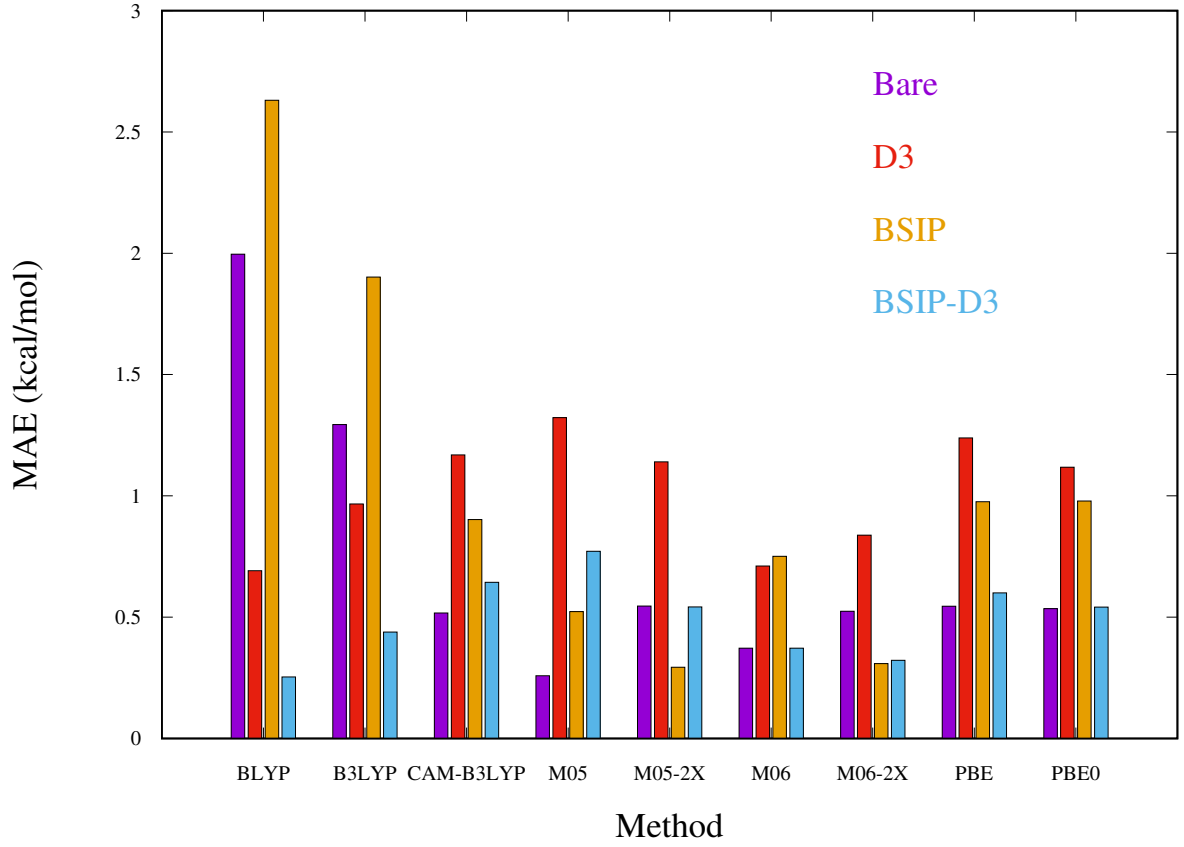


Figure 5: Mean absolute errors for a diverse set of DFT functionals using 6-31+G** as basis sets with respect to our benchmark binding energies. MAE $= \frac{1}{N}\sum |\mathrm{BE}_{\mathrm{ave}}^{\mathrm{DZ-TZ}} - \mathrm{BE}_{\mathrm{DFT}}|$, $N$ runs for all the 2376 complexes. The legends D3 (red) and BSIP (orange) represent the use of empirical dispersion and basis set incompleteness potentials. The legend BSIP-D3 (cyan) is the combined use of the previous two and Bare (purple) the absence of both.

# 3 Results and Discussion

A diverse set of water cluster-probe configurations was obtained from the process described in the previous section. Figure 6 shows all benchmark binding energies (BE) obtained for the dimethyl ether molecule and all of the different water clusters. Due to its relatively simple structure, the discussion will be focused on this probe. The BE data cover an energy range from -0.19 kcal/mol to -8.42 kcal/mol. A careful inspection of the geometries of the complexes associated with Figure 6 led us to identify six different classifications of noncovalent interactions, summarized and defined in Figure 7. This classification can be extended to the rest of the complexes formed with all probes. Analogous graphs for the remainder of the organic molecules can be found in the SI. They all display a similar pattern and the same type of noncovalent interactions. The only exception is dimethylamine, which presents an additional interaction when the probe donates an HB (N−H) to an oxygen atom in a water cluster; this interaction is usually found to contribute ca. -2 kcal/mol to -3 kcal/mol to the BE.

The noncovalent interaction **A**, portrayed in Figure 7, can occur with, and increase the strengths of, other types of interactions, especially the **DDDA** and **DDSA** types. The majority of **A+DDDA** and **A+DDSA** interactions are obtained in larger clusters; in most cases, the water clusters larger than the trimer are able to accommodate secondary interactions between aliphatic hydrogens and the water cluster. However, in some cases, an **A+SDSA** type complex can be observed, as shown in Figure 8. Plotting the benchmark BE using this classification of noncovalent interactions results in Figure 9. From this graph, and taking the most stable complex in each case, type **A** emerges as the weakest of the probe-water complex interactions because it involves primarily dipole-dipole interactions and C−H $\cdots$ $(H_2O)_n$ dispersion interactions. For the HBs present in the monomer and dimer clusters, the following order of BE strength is observed: **DD**<**Monomer**<**SDSA**<**A+SDSA**. The weakest of these interactions is the **DD** since it forms a hydrogen bond with the organic probe through a water acting as a double HB donor. As Figure 7 depicts, the water donating an HB

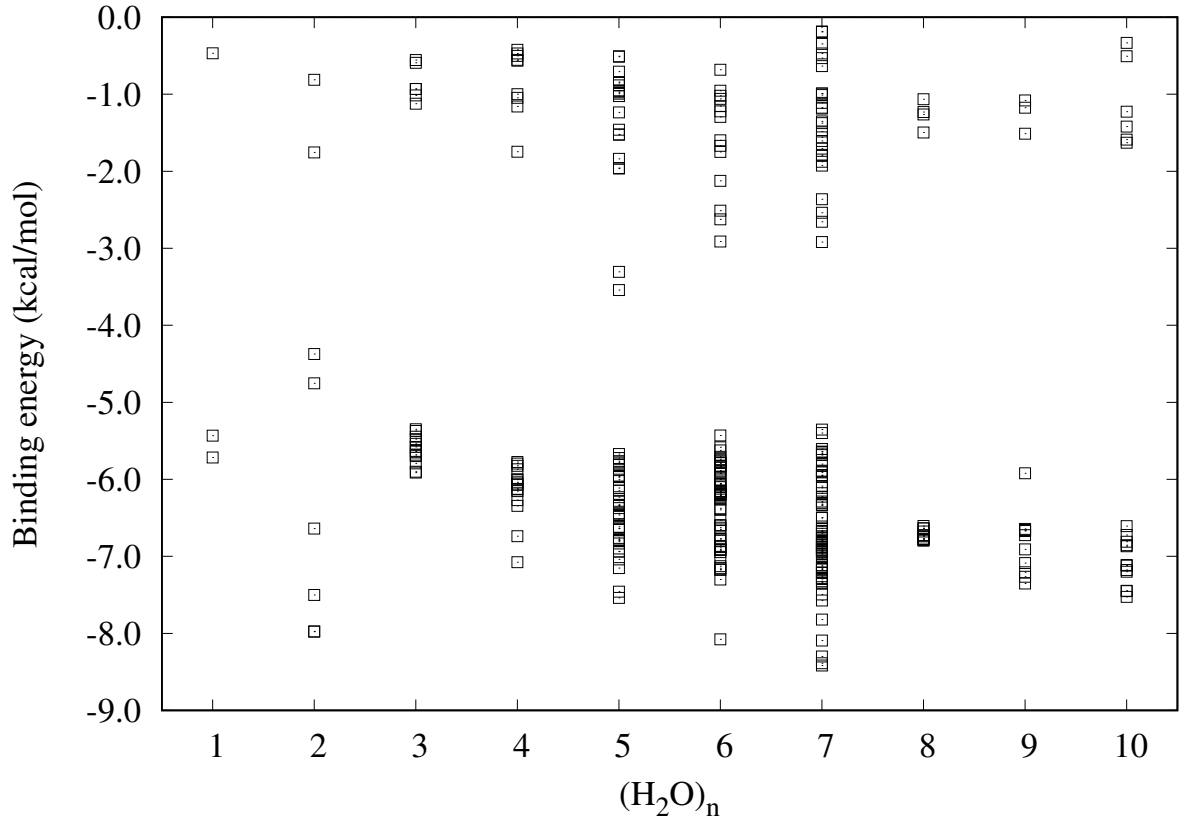


Figure 6: Profile of all binding energies for dimethyl ether and $(H_2O)_n$ (with n = 1-10) at our benchmark level of theory.

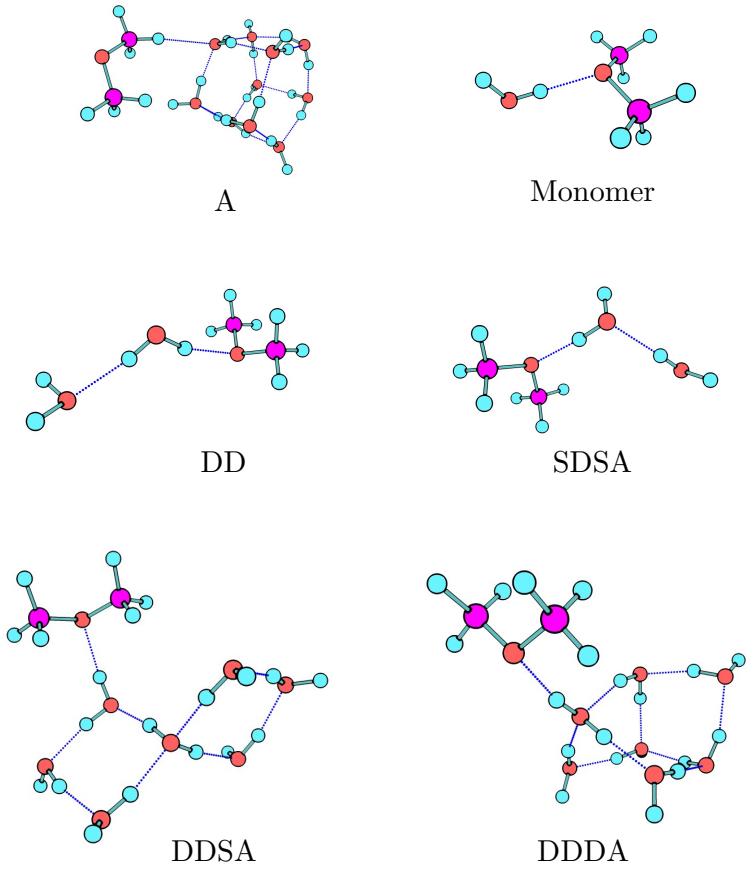


Figure 7: The **A** label represents all weak interactions that do not involve an $-$OH group from the water clusters donating an HB to the probes; dispersion, dipole-dipole, and $C-H\cdots(H_2O)_n$ interactions are included in this type of bonding. The **Monomer** type corresponds to the $H_2O$ molecule donating a hydrogen bond to the heteroatoms in the probes. In the case of the water dimer (2Cs), there are two possibilities: **DD** when the water molecule is a double HB donor (one HB donated to the probe and one donated to another water), and **SDSA** if it is both a single donor (HB to the probe) and an acceptor of an HB (from a water). There are only two types of HB from the trimer to the decamer: **DDSA**, in which the water molecule donating to the organic probe is a double donor and a single acceptor of HB, and **DDDA** where a water acts as a double HB donor and double acceptor. Colour code, red: oxygen, blue: hydrogen, and magenta: carbon. Dashed lines indicate either HB or $C-H\cdots(H_2O)_n$ interactions.

to the organic probe is also donating an HB to a neighbouring molecule of water: accepting electronic density from both molecules and reducing the HB donating capabilities of the central water in **DD**. For **SDSA** and **A+SDSA**, the water molecule donating an HB to the probe is also acting as an HB acceptor of another water molecule. This is the well-known "cooperative" effect in hydrogen bonding: The water bound to the probe is electron deficient because it is donating electron density to a neighbouring water molecule, making the former water better able to accept electron density from the probe. This effect is also at play in the **A+SDSA** motif, which interactions are further enhanced by the secondary **A** interactions. The monomer, which lacks neighbour water molecules acting as HB acceptors or donors, falls between the two dimer cases.

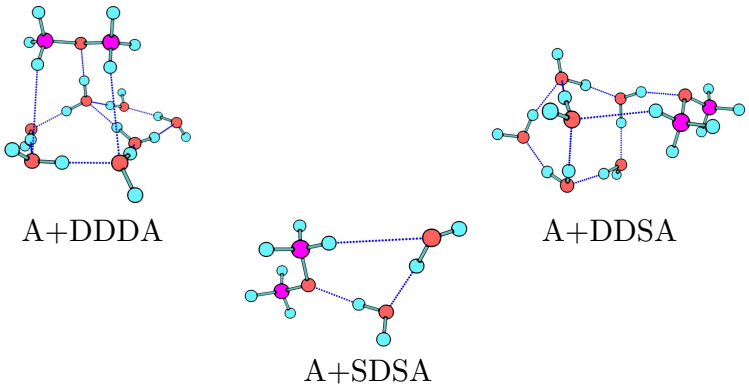


Figure 8: Some of the noncovalent bonds defined in Figure 7 can gain additional stability when combined with type **A** interactions. Colour code, red: oxygen, blue: hydrogen, and magenta: carbon. Dashed lines indicate either HB or $C-H\cdots(H_2O)_n$ interactions.

For the water clusters ranging in size from the trimer to the decamer, Figure 8 shows the following order of BE strength: **DDSA** < **DDDA** < **A+DDSA** < **A+DDDA**. In these cases, all interactions involve a water acting as a double hydrogen bond donor to a different water and the organic probe, and the water accepting a single HB from a neighbouring water (**DDSA**) or the water accepting two HBs from two neighbouring waters (**DDDA**). For the same arguments given in the dimer example, a water molecule accepting more HBs from neighbouring waters is a better HB donor than one accepting fewer HBs, therefore **DDDA** motifs result in stronger BEs than **DDSA**. Likewise, **A+DDDA** represents a more

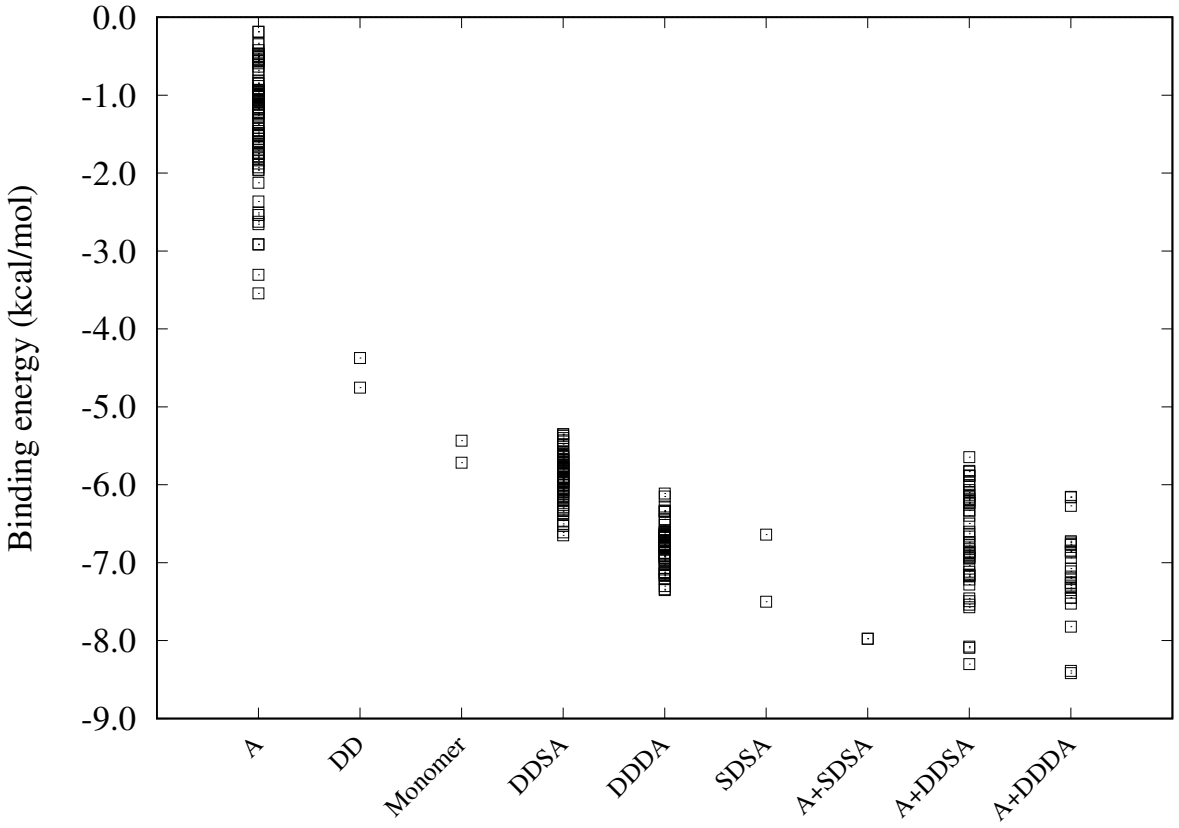


Figure 9: Benchmark-level binding energies for dimethyl ether and $(H_2O)_n$ (with n = 1-10) classified according to figures 7 and 8.

stable interaction with respect to **A+DDSA**, with extra stability due to the secondary interactions. Similar hierarchies, based on the donating and acceptor capabilities of water, have been proposed in the past to classify hydrogen bonds within water clusters.[25,26]

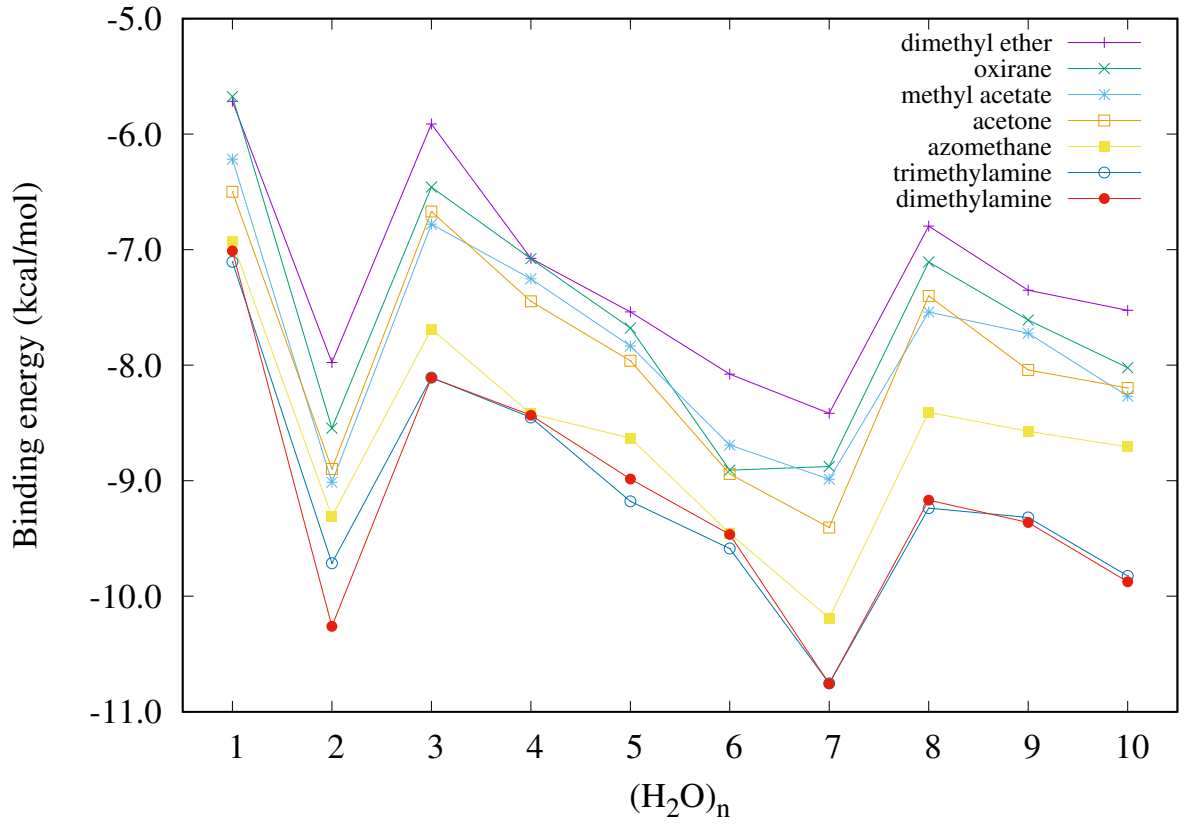


Figure 10: $BE_{ave}^{DZ-TZ}$ profile for the most stable complexes of each of the studied organic molecules with the water clusters.

Examining the most stable complex of each water cluster with each of the organic probes shows that the profile of benchmark binding energies (Figure 10) has an irregular trend with increasing n in $(H_2O)_n$ without appearing to reach an asymptote by n=10. To explain this trend in the curves, we noted that the water cluster displaying the strongest HB interactions belongs to the water heptamer - this it is the largest water cluster presenting book-like geometries, which allow for **A+DDDA** type interactions. Of the 11 heptamer structures we obtained from the literature,[31] 6 are open structures (i.e. they do not form cages or prisms) which allow for **A** type interactions in addition to **DDDA** interactions. In contrast, the

Table 2: Benchmark binding energies of the most stable complexes between heptamers and all probes. All values are in kcal/mol and sorted from weakest to strongest interaction.

| Probe | $BE_{ave}^{DZ-TZ}$ (kcal/mol) |
|---|---|
| Dimethyl ether | -8.42 |
| Oxirane | -8.88 |
| Methyl acetate | -8.99 |
| Acetone | -9.41 |
| Azomethane | -10.19 |
| Trimethylamine | -10.75 |
| Dimethylamine | -10.76 |

octamer, nonamer, and decamer's geometries include only 6 geometries in total, all of which have cage-like structures in which further stabilization via **A** interactions is absent or not optimal. Figure 11 illustrate this using complexes formed between $(H_2O)_n$ and dimethylamine. These findings suggest to us that the magnitude of the BEs obtained with the heptamer are likely to be quite close to the maximum HB strengths between the probes and water clusters.

The nature of the organic probe is also an important determinator of HB binding strengths. Table 2 displays the benchmark binding energies for the most stable heptamer complexes per organic molecule; the data shows that the nitrogen-based probes produce the more stable complexes of the set. The calculated BEs follow the trend expected on the basis of Abraham's HB basicity scale,[66,67] $\beta_2^H$. Abraham's scale places non-basic compounds, such as alkanes, at zero and more basic molecules at higher values. Table 3 shows that nitrogen-containing molecules are more basic than oxygen-based probes, which indicates that nitrogen is a better HB acceptor than oxygen. For dimethyl ether, oxirane, methyl acetate, and acetone with BEs of -8.42, -8.88, -8.99, and -9.41 kcal/mol, respectively, the $\beta_2^H$ values increase monotonically over the series from 0.40 to 0.50. For the nitrogen-containing probes azomethane, trimethylamine, and dimethylamine, with BEs of -10.19, -10.75, and -10.76 kcal/mol respectively, the $\beta_2^H$ are 0.64 (using pyridazine to represent azomethane), 0.67 (using $Et_3N$), and 0.70 (using $Et_2NH$).

Finally, the benchmark binding energies per individual clusters for the dimethyl ether

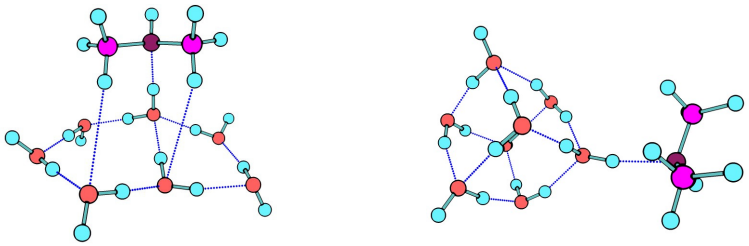

7CH3 - dimethylamine
complex (A+DDDA)
BE = -10.76 kcal/mol

8S4 - dimethylamine
complex (DDDA)
BE = -9.17 kcal/mol

Figure 11: The formation of the shown complex between cluster 7CH3 and dimethylamine leads to the strongest binding energy of all; the strong interaction occurs via a **DDDA** interaction that is stabilized by **A** interactions. The strongest interaction among octamers and dimethylamine is also displayed; there is no additional **A** stabilization for this case. Colour code, red: oxygen, blue: hydrogen, magenta: carbon, and maroon: nitrogen. Dashed lines indicate either HB or $C-H\cdots(H_2O)_n$ interactions.

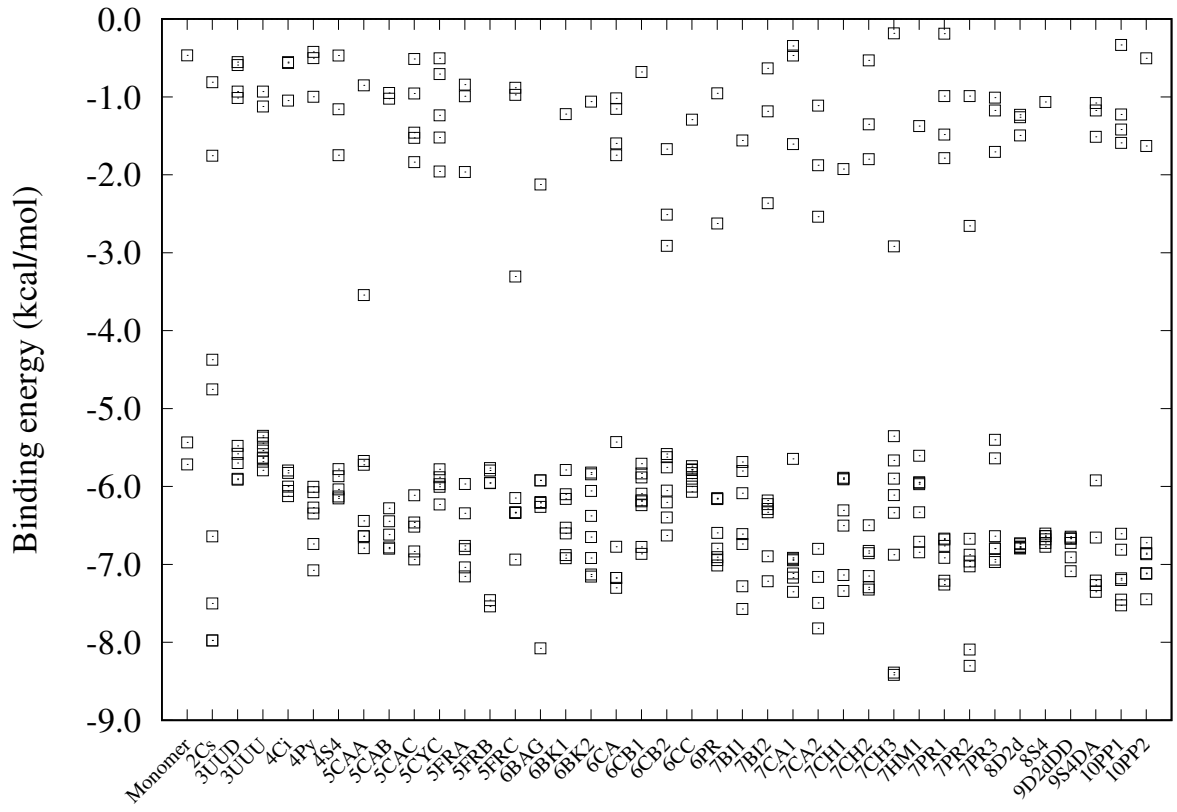


Figure 12: Benchmark binding energies for dimethyl ether and individual clusters as labelled in Table 1.

Table 3: Abraham's parameters for HB basicity of selected organic molecules corresponding to our probes or structurally comparable compounds. The data was obtained from references 66 and 67.

| Molecule | Comparable to | $\beta_2^{\mathrm{H}}$ |
|---|---|---|
| Diethyl ether | Dimethyl ether | 0.45 |
| Di-*n*-propyl ether | Dimethyl ether | 0.45 |
| Di-*n*-butyl ether | Dimethyl ether | 0.45 |
| THF | Oxirane | 0.48 |
| Methyl acetate | - | 0.45 |
| Acetone | - | 0.49 |
| Pyridazine | Azomethane | 0.64 |
| Trimethylamine | - | 0.67 |
| Dimethylamine | - | 0.66 |

probe (Figure 12) show a similar distribution of the BE from the pentamer to the decamer. Some complexes for the 6BAG, 7CH3, and 7PR2 clusters present geometries that are more stable than the rest structures; this situation can be explained in terms of **A** stabilization. Again, since the $(H_2O)_{8\text{-}10}$ systems are all cage-like, the **A** stabilization is not present or not as favourable as in the open water cluster structures. Setting aside the methyl acetate, which is the less symmetrical and the most structurally complex of the probes, all organic molecules show a similar distribution of binding energies (see also the additional data presented in the SI). We can expect that AOC reactions involving the moieties present in our probes would behave similarly when interacting with water molecules. We imagine real water-organic reactions involving significant dynamics in HB formation between the probes and the water systems with which they interact resulting in fluctuations in BE over time. We suspect that the maximum strength of the BEs achievable will likely be quite close those calculated for the probe-$(H_2O)_7$. Of course, entropy effects will impact the nature of the complexes formed in real systems.

# 4 Conclusions

Understanding noncovalent interactions between organic molecules and water clusters is required in order to understand the chemistry of aqueous organic phenomena. Secondary interactions play a critical role in forming organic molecule-water cluster complexes. While contact between a heteroatom in the organic probe and a −OH group from the cluster is required for a strong interaction, additional interactions from aliphatic hydrogens can provide extra stabilization to the complexes. We showed that the nature of the water molecule interacting with the organic species, whether it is acting as a single or double HB acceptor or donor, determines the strength of binding energies of the complexes. The nature of the organic probe is also an important determinant of HB strengths. Therefore, the computational study of AOC reactions requires consideration of the size of the water cluster and the nature of the secondary interactions, the HB donors and acceptors, and that of the organic molecules. The presence of different moieties in the probes can lead to a more complex distribution of the BEs; for instance, methyl acetate can engage in many of the classes of interactions identified in this work. Overall, our work illustrates the intricate nature of reactions in aqueous phase. This work also provides a novel benchmark data set for organic probe-water cluster binding energies that can be used, for example, in the assessment of computational methods that describe noncovalent interactions.

# 5 Acknowledgements

GAD acknowledges the Canada Foundation for Innovation, the National Science and Engineering Research Council, and the British Columbia Knowledge Development Fund for funding. ERM thanks Zhipeng Pei for providing technical support in the use of the MOLCLUS software. ERM is also thankful to CONACyT for the scholarship 308773/472432.

# 6 Supporting Information Available

Binding energy plots for acetone, oxirane, methyl acetate, azomethane, dimethylamine, and trimethylamine, as well as XYZ coordinates for all structures, CBS graphs, and detailed DFT and benchmark data are available free of charge at http://pubs.acs.org.

# References


(1) Diels, O.; Alder, K. Synthesen in der hydroaromatische reihe. *Justus Liebigs Ann. Chem.* **1931**, *490*, 243–257.

(2) Rideout, D. C.; Breslow, R. Hydrophobic acceleration of Diels-Alder reactions. *J. Am. Chem. Soc.* **1980**, *102*, 7816–7817.

(3) Breslow, R.; Maitra, U.; Rideout, D. Selective Diels-Alder reactions in aqueous solutions and suspensions. *Tetrahedron Lett.* **1983**, *24*, 1901–1904.

(4) Breslow, R. Hydrophobic effects on simple organic reactions in water. *Acc. Chem. Res.* **1991**, *24*, 159–164.

(5) Breslow, R. Determining the geometries of transition states by use of antihydrophobic additives in water. *Acc. Chem. Res.* **2004**, *37*, 471–478.

(6) Kitanosono, T.; Masuda, K.; Xu, P.; Kobayashi, S. Catalytic organic reactions in water toward sustainable society. *Chem. Rev.* **2018**, *118*, 679–746.

(7) Kitanosono, T.; Kobayashi, S. Reactions in water involving the "on-water" mechanism. *Chem. Eur. J.* **2020**, 1–23.

(8) Simon, M. O.; Li, C. J. Green chemistry oriented organic synthesis in water. *Chem. Soc. Rev.* **2012**, *41*, 1415–1427.

(9) Lipshutz, B. H.; Ghorai, S. Transitioning organic synthesis from organic solvents to water. What's your E factor? *Green Chem.* **2014**, *16*, 3660–3679.

(10) Lipshutz, B. H.; Gallou, F.; Handa, S. Evolution of solvents in organic chemistry. *ACS Sustain. Chem. Eng.* **2016**, *4*, 5838–5849.

(11) Anastas, P. T.; Kirchhoff, M. M. Origins, current status, and future challenges of green chemistry. *Acc. Chem. Res.* **2002**, *35*, 686–694.

(12) Jung, Y.; Marcus, R. A. On the theory of organic catalysis "on water". *J. Am. Chem. Soc.* **2007**, *129*, 5492–5502.

(13) Oberbeck, V. R.; Marshall, J.; Shen, T. Prebiotic chemistry in clouds. *J. Mol. Evol.* **1991**, *32*, 296–303.

(14) Benner, S. A.; Kim, H. J.; Carrigan, M. A. Asphalt, water, and the prebiotic synthesis of ribose, ribonucleosides, and RNA. *Acc. Chem. Res.* **2012**, *45*, 2025–2034.

(15) Stroberg, W.; Schnell, S. Do cellular condensates accelerate biochemical reactions? Lessons from microdroplet chemistry. *Biophys. J.* **2018**, *115*, 3–8.

(16) Nakanishi, K. The chemistry of brevetoxins: a review. *Toxicon* **1985**, *23*, 473–479.

(17) Vilotijevic, I.; Jamison, T. F. Epoxide-opening cascades promoted by water. *Science* **2007**, *317*, 1189–1192.

(18) Morten, C. J.; Byers, J. A.; Jamison, T. F. Evidence that epoxide-opening cascades promoted by water are stepwise and become faster and more selective after the first cyclization. *J. Am. Chem. Soc.* **2011**, *133*, 1902–1908.

(19) Nishikawa, K.; Morita, K.; Hashimoto, S.; Hoshino, A.; Ikeuchi, T.; Kumagai, M.; Morimoto, Y. Critical switching of cyclization modes of polyepoxides in acidic aqueous media and neutral water: synthesis and revised structure of a nerolidol-type sesquiterpenoid. *Angew. Chem. Int. Ed.* **2019**, *58*, 10168–10172.

(20) Mó, O.; Yáñez, M.; Elguero, J. Cooperative (nonpairwise) effects in water trimers: an ab initio molecular orbital study. *J. Chem. Phys.* **1992**, *97*, 6628–6638.

(21) Glendening, E. D. Natural energy decomposition analysis: extension to density functional methods and analysis of cooperative effects in water clusters. *J. Phys. Chem. A* **2005**, *109*, 11936–11940.

(22) Ohno, K.; Okimura, M.; Akai, N.; Katsumoto, Y. The effect of cooperative hydrogen bonding on the OH stretching-band shift for water clusters studied by matrix-isolation infrared spectroscopy and density functional theory. *Phys. Chem. Chem. Phys.* **2005**, *7*, 3005–3014.

(23) Pérez, C.; Zaleski, D. P.; Seifert, N. A.; Temelso, B.; Shields, G. C.; Kisiel, Z.; Pate, B. H. Hydrogen bond cooperativity and the three-dimensional structures of water nonamers and decamers. *Angew. Chem. Int. Ed.* **2014**, *53*, 14368–14372.

(24) Guevara-Vela, J. M.; Chávez-Calvillo, R.; García-Revilla, M.; Hernández-Trujillo, J.; Christiansen, O.; Francisco, E.; Pendás, Á. M.; Rocha-Rinza, T. Hydrogen-bond cooperative effects in small cyclic water clusters as revealed by the interacting quantum atoms approach. *Chem. Eur. J.* **2013**, *19*, 14304–14315.

(25) Guevara-Vela, J. M.; Romero-Montalvo, E.; Mora Gómez, V. A.; Chávez-Calvillo, R.; García-Revilla, M.; Francisco, E.; Pendás, Á. M.; Rocha-Rinza, T. Hydrogen bond cooperativity and anticooperativity within the water hexamer. *Phys. Chem. Chem. Phys.* **2016**, *18*, 19557–19566.

(26) Castor-Villegas, V. M.; Guevara-Vela, J. M.; Vallejo Narváez, W. E.; Martín Pendás, Á.; Rocha-Rinza, T.; Fernández-Alarcón, A. On the strength of hydrogen bonding within water clusters on the coordination limit. *J. Comput. Chem.* **2020**, *41*, 2266–2277.

(27) Domingo, L.; Saéz, J.; Zaragozá, R.; Arnó, M. Understanding the participation of

quadricyclane as nucleophile in polar $[2\sigma + 2\sigma + 2\pi]$ cycloadditions toward electrophilic $\pi$ molecules. *J. Org. Chem.* **2008**, *73*, 8791–8799.

(28) Kong, S.; Evanseck, J. D. Density functional theory study of aqueous-phase rate acceleration and endo/exo selectivity of the butadiene and acrolein Diels-Alder Reaction. *J. Am. Chem. Soc.* **2000**, *122*, 10418–10427.

(29) Fanourgakis, G. S.; Apra, E.; de Jong, W. A.; Xantheas, S. S. the four low-lying families of minima of . II . Spectroscopic signatures of the dodecahedron , fused cubes , face-sharing pentagonal prisms , and edge-sharing pentagonal prisms hydrogen bonding networks and edge-sharing pentagonal prisms hydrogen bonding. *J. Chem. Phys.* **2005**, *122*, 134304.

(30) Miliordos, E.; Aprà, E.; Xantheas, S. S. Optimal geometries and harmonic vibrational frequencies of the global minima of water clusters $(H_2O)_n$, n=2–6, and several hexamer local minima at the CCSD(T) level of theory Optimal geometries and harmonic vibrational frequencies of the global. *J. Chem. Phys.* **2013**, *139*, 114302.

(31) Temelso, B.; Archer, K. A.; Shields, G. C. Benchmark structures and binding energies of small water clusters with anharmonicity corrections. *J. Phys. Chem. A* **2011**, *115*, 12034–12046.

(32) Feyereisen, M.; Fitzgerald, G.; Komornicki, A. Use of approximate integrals in ab initio theory. An application in MP2 energy calculations. *Chem. Phys. Lett.* **1993**, *208*, 359–363.

(33) Bernholdt, D. E.; Harrison, R. J. Large-scale correlated electronic structure calculations: the RI-MP2 method on parallel computers. *Chem. Phys. Lett.* **1996**, *250*, 477–484.

(34) Kendall, R. A.; Dunning, T. H.; Harrison, R. J. Electron affinities of the first-row

atoms revisited. Systematic basis sets and wave functions. *J. Chem. Phys.* **1992**, *96*, 6796–6806.

(35) Becke, A. D. Density-functional thermochemistry. III. The role of exact exchange. *J. Chem. Phys.* **1993**, *98*, 5648–5652.

(36) Lee, C.; Yang, W.; Parr, R. G. Development of the Colle-Salvetti correlation-energy formula into a functional of the electron density. *Phys. Rev. B* **1988**, *37*, 785–789.

(37) Stephens, P. J.; Devlin, F. J.; Chabalowski, C. F.; J, F. M. Ab initio calculation of vibrational absorption and circular dichroism spectra using density functional force fields. *Journal of Physical Chemistry* **1994**, *98*, 11623–11627.

(38) Frisch, M. J. et al. Gaussian 16 Revision C.01. 2016; Gaussian Inc. Wallingford CT.

(39) Chanda, A.; Fokin, V. V. Organic synthesis "on water". *Chem. Rev.* **2009**, *109*, 725–748.

(40) Lu, T. Molclus Program, Version 1.8.4. http://www.keinsci.com/research/molclus.html (accessed June 25, 2019).

(41) Rappe, A. K.; Casewit, C. J.; Colwell, K. S.; Goddard, W. A.; Skiff, W. M. UFF, a full periodic table force field for molecular mechanics and molecular dynamics simulations. *J. Am. Chem. Soc.* **1992**, *114*, 10024–10035.

(42) Prasad, V. K.; Otero-de-la Roza, A.; DiLabio, G. A. Atom-Centered potentials with dispersion-corrected minimal-basis-set Hartree–Fock: an efficient and accurate computational approach for large molecular systems. *J. Chem. Theory Comput.* **2018**, *14*, 726–738.

(43) Otero-de-la Roza, A.; DiLabio, G. A. Transferable atom-centered potentials for the correction of basis set incompleteness errors in density-functional theory. *J. Chem. Theory Comput.* **2017**, *13*, 3505–3524.

(44) Grimme, S.; Antony, J.; Ehrlich, S.; Krieg, H. A consistent and accurate ab initio parametrization of density functional dispersion correction (DFT-D) for the 94 elements H-Pu. *J. Chem. Phys.* **2010**, *132*, 154104.

(45) Grimme, S.; Ehrlich, S.; Goerigk, L. Effect of the damping function in dispersion corrected density functional theory. *J. Comput. Chem.* **2011**, *32*, 1456–1465.

(46) Becke, A. D.; Johnson, E. R. A density-functional model of the dispersion interaction. *J. Chem. Phys.* **2005**, *123*, 154101.

(47) Johnson, E. R.; Becke, A. D. A post-Hartree-Fock model of intermolecular interactions: inclusion of higher-order corrections. *J. Chem. Phys.* **2006**, *124*, 174104.

(48) Otero-de-la Roza, A.; Blanco, M. A.; Pendás, A. M.; Luaña, V. Critic: a new program for the topological analysis of solid-state electron densities. *Comput. Phys. Commun.* **2009**, *180*, 157–166.

(49) Otero-de-la Roza, A.; Johnson, E. R.; Luaña, V. Critic2: a program for real-space analysis of quantum chemical interactions in solids. *Comput. Phys. Commun.* **2014**, *185*, 1007–1018.

(50) Chemcraft - graphical software for visualization of quantum chemistry computations. https://www.chemcraftprog.com.

(51) Riplinger, C.; Neese, F. An efficient and near linear scaling pair natural orbital based local coupled cluster method. *J. Chem. Phys.* **2013**, *138*, 034106.

(52) MacKie, I. D.; DiLabio, G. A. Approximations to complete basis set-extrapolated, highly correlated non-covalent interaction energies. *J. Chem. Phys.* **2011**, *135*, 134318.

(53) Davidson, E. R.; Chakravorty, S. J. A possible definition of basis set superposition error. *Chem. Phys. Lett.* **1994**, *217*, 48–54.

(54) Boys, S. F.; Bernardi, F. The calculation of small molecular interactions by the differences of separate total energies. Some procedures with reduced errors. *Mol. Phys.* **1970**, *19*, 553–566.

(55) Neese, F. The ORCA program system. *WIREs Comput. Mol. Sci.* **2012**, *2*, 73–78.

(56) Martin, J. M. L. Ab initio total atomization energies of small molecules — towards the basis set limit. *Chem. Phys. Lett.* **1996**, *259*, 669–678.

(57) Becke, A. D. Density-functional exchange-energy approximation with correct asymptotic behavior. *Phys. Rev. A* **1988**, *38*, 3098–3100.

(58) Yanai, T.; Tew, D. P.; Handy, N. C. A new hybrid exchange–correlation functional using the Coulomb-attenuating method (CAM-B3LYP). *Chem. Phys. Lett.* **2004**, *393*, 51–57.

(59) Zhao, Y.; Schultz, N. E.; Truhlar, D. G. Exchange-correlation functional with broad accuracy for metallic and nonmetallic compounds, kinetics, and noncovalent interactions. *J. Chem. Phys.* **2005**, *123*, 161103.

(60) Zhao, Y.; Schultz, N. E.; Truhlar, D. G. Design of density functionals by combining the method of constraint satisfaction with parametrization for thermochemistry, thermochemical kinetics, and noncovalent interactions. *J. Chem. Theory Comput.* **2006**, *2*, 364–382.

(61) Zhao, Y.; Truhlar, D. G. The M06 suite of density functionals for main group thermochemistry, thermochemical kinetics, noncovalent interactions, excited states, and transition elements: two new functionals and systematic testing of four M06-class functionals and 12 other functionals. *Theor. Chem. Acc.* **2008**, *120*, 215–241.

(62) Perdew, J. P.; Burke, K.; Ernzerhof, M. Generalized gradient approximation made simple. *Phys. Rev. Lett.* **1997**, *78*, 1396–1396.

(63) Perdew, J. P.; Burke, K.; Ernzerhof, M. Generalized gradient approximation made simple. *Phys. Rev. Lett.* **1996**, *77*, 3865–3868.

(64) Adamo, C.; Barone, V. Toward reliable density functional methods without adjustable parameters: the PBE0 model. *J. Chem. Phys.* **1999**, *110*, 6158–6170.

(65) Ernzerhof, M.; Scuseria, G. E. Assessment of the Perdew–Burke–Ernzerhof exchange-correlation functional. *J. Chem. Phys.* **1999**, *110*, 5029–5036.

(66) Abraham, M. H.; Grellier, P. L.; Prior, D. V.; Morris, J. J.; Taylor, P. J. Hydrogen bonding. Part 10. A scale of solute hydrogen-bond basicity using log K values for complexation in tetrachloromethane. *J. Chem. Soc. Perkin Trans.* **1990**, *2*, 521–529.

(67) Abraham, M. H. Scales of solute hydrogen-bonding: their construction and application to physicochemical and biochemical processes. *Chem. Soc. Rev.* **1993**, *22*, 73–83.

# Computational study of hydrogen bond interactions in water cluster-organic molecule complexes

Eduardo Romero-Montalvo[†] and Gino DiLabio[*,†,‡]

†*Department of Chemistry, University of British Columbia, 3247 University Way, Kelowna, British Columbia, Canada V1V 1V7*

‡*Faculty of Management, University of British Columbia, 1137 Alumni Avenue, Kelowna, British Columbia, Canada V1V 1V7*

E-mail: gino.dilabio@ubc.ca

## Table of contents graphic

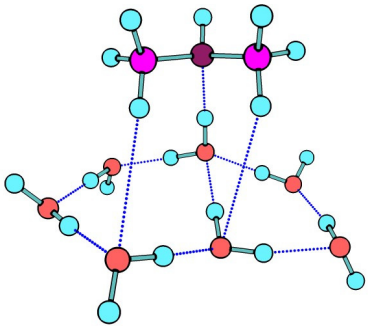

7CH3 - dimethylamine
complex (A+DDDA)
BE = -10.76 kcal/mol

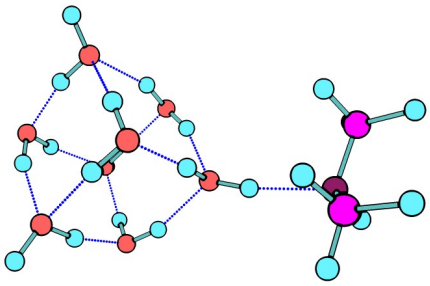

8S4 - dimethylamine
complex (DDDA)
BE = -9.17 kcal/mol